Materials Research. 2024; 27:e20240124
DOI: https://doi.org/10.1590/1980-5373-MR-2024-0124

Polyethylene of Raised Temperature Resistance (PE-RT) Nanocomposites Reinforced with Graphene Oxide for Application in Flexible Pipelines

***Barbara de Salles Macena da Cruz*[a], *Lucas Galhardo Pimenta Tienne*[a], *Elen da Silva Santos*[a], *Fábio Elias Jorge*[a], *Maria de Fátima Vieira Marques*[a*], *Erica Gervasoni Chaves*[b]**

[a]*Universidade Federal do Rio de Janeiro, Instituto de Macromoléculas Professora Eloisa Mano, Av. Horácio Macedo, 2090, 21941-598, Rio de Janeiro, RJ, Brasil.*
[b]*Petrobras, Centro de Pesquisas, Desenvolvimento e Inovação Leopoldo Américo Miguez de Mello, Ilha do Fundão, Av. Horácio Macedo, 950, 21941-915, Rio de Janeiro, RJ, Brasil.*

Received: March 18, 2024; Revised: June 04, 2024; Accepted: July 16, 2024

Polyethylene of Raised Temperature Resistance (PE-RT) is a specially designed high-density polyethylene utilizing bimodal resin technology. It is suitable for oil and gas pipeline applications, exhibiting excellent long-term creep resistance at elevated temperatures. Flexible risers require security against potential offshore oil leaks, prompting the reinforcement of PE-RT with graphene oxide (GO) at concentrations of 0.5, 1.0, and 2.0 wt.%. The nanocomposites were processed in a twin-screw mini extruder at 180°C, with a screw speed of 100 rpm and a residence time of 6 min. The results indicated an increase in the thermal stability of the nanocomposite by 14°C. XRD and DSC analyses revealed a higher crystallinity index for the sample with the lowest GO content. The water contact angle values increased from 98° in the pure matrix to 102° in the nanocomposite, suggesting a slight increase in the material's hydrophobicity due to nanoparticle incorporation. SEM images demonstrated a good interface between GO nanoparticles and PE-RT without agglomeration. The Shore D hardness increased from 50 to 59 with 2.0 wt.% GO. Although the 0.5 wt.% GO composition exhibited a higher degree of crystallinity, other properties such as thermal resistance, Shore D hardness, contact angle, dispersion, and homogeneity tended to improve with increasing nanoparticle content. Consequently, it can be concluded that the optimal concentration of GO in the PE-RT matrix is approximately 1.0 wt.%. Incorporating 1.0 wt.% GO resulted in an increase in Young's modulus from 335 ± 37 MPa to 409 ± 42 MPa, indicating enhanced mechanical strength of PE-RT. Finally, aging tests showed that GO reduced the swelling degree of the final material, suggesting that PE-RT/GO is a promising candidate for pipeline applications.

Keywords: *Polyethylene of Raised Temperature Resistance (PE-RT), graphene oxide, nanocomposites, nanotechnology.*

1. Introduction

Flexible pipelines, also called risers, are used to transport oil from the well to production systems, as well as to transfer production to processing units[1]. They are made of on-adherent polymeric and metallic layers, each responsible for a specific structural function. Sheet metal can suffer from a failure mechanism known as fatigue corrosion, caused by seawater entry into the pipeline's annulus, initiated by any damage to the outer layer and/or the transport of condensed water and contaminants received through the pipeline[2]. Crude oil contains various corrosive contaminants such as CO_2 and H_2S, which, together with displacement caused by current and cyclic waves in the flexible riser, can lead to resistance fatigue, with cracks and collapses[3]. In flexible pipelines, the polymeric barrier layer must be leakproof, which is an essential requirement. Any damage to the barrier that permits oil to leak into the external environment can result in serious environmental disasters, most of which are irreparable[4]. Non-adherent flexible pipelines are designed following the specification of the main requirement to be met by the barrier layer, which is to maintain the tightness capacity throughout the useful life of the pipeline, generally corresponding to 25 years[5]. High-density polyethylene (HDPE) is one of the most widely used polymeric materials as a component of petroleum risers, especially employed in low-pressure and temperature conditions due to its moderate thermal stability, excellent chemical/oxidation resistance, and hydrophobicity[6,7].

According to the literature[5-7], it is plausible to anticipate that the polymeric layer of pipelines may experience swelling due to exposure to the transported materials. This swelling can potentially lead to the complete collapse of the tube, primarily because the polymeric layer may be unable to expand freely due to external constraints imposed by the surrounding steel layers. Swelling can cause a severe decrease in the mechanical properties of polymeric materials, weakening the structural stability of the entire pipeline.

*e-mail: fmarques@ima.ufrj.br

The major limitation of polyethylenes, in general, is that when in contact with non-polar solvents, they undergo swelling, partial dissolution, modification of their original color, and, over time, loss of properties occurs, resulting in a reduction in the mechanical resistance of the material, due to the effect of surface tension cracking[8]. Kong and collaborators[9] investigated a collapsed tube, concluding through shore D hardness tests and thermogravimetric analysis that the collapse occurred due to the combination of swelling and exposure to high working temperature (90 °C), proving that these two factors are mainly responsible for the limitation of polyethylenes as a polymeric barrier layer material.

Polyethylene of Raised Temperature Resistance (PE-RT), a special type of HDPE, can be classified into two types: I and II. Type II has a higher density and offers better resistance to high temperature and pressure compared to Type I[9]. The two primary processes for producing PE-RT are solution polymerization, developed by Dow Chemical Company, and bulk polymerization, industrialized by Basell Company. It is designed with bimodal resin technology. It can involve either a single reactor containing two different catalysts in the solution process or two reactors in series in the gas-phase process. This technology produces PE-RT resin with two very different molecular mass fractions, achieving excellent performance at elevated temperatures[10]. It contains a greater fraction of high molar mass chains compared to other polyethylenes, resulting in enhanced properties and durability[11]. In addition, the long-term strength, toughness, ductility, resistance to fatigue, and the ability for PE-RT pipe to be cold-bent in the field, eliminating many elbow connections, make this material stand out in a different light[1].

PE-RT is a copolymer of ethylene and α-olefin, where the α-olefins commonly used are C3 (propylene), C4 (1-butene), C6 (1-hexene) and C8 (1-octene)[2]. Ethylene-α-olefin copolymers are important products with favorable properties and are good alternatives to ethylene homopolymers. Incorporating relatively low amounts of α-olefin comonomer in the polyethylene changes the crystalline structure of the final product due to the addition of short chains pendant in the polymer backbone[3]. An improvement in resistance to environmental stress cracking (ESCR) is observed by the increased concentration of tie molecules since imperfections are created in the crystalline structure of the polymer by the short branching, excluding long chains from the lamellae[4,12]. Therefore, lamellar crystalline structures are interconnected through amorphous tie molecule segments. The likelihood of forming these binding chains increases as the tie molecule's length becomes greater[6,12]. As it forms a tie between the crystals, it greatly increases their thermal resistance. In fact, these tie molecules increase the material's useful life due to the connection between several crystals, exhibiting extensibility and mobility, absorbing and dissipating energy, increasing toughness and long-term fracture resistance[7].

Therefore, PE-RT is widely used in hot water piping systems because of its high-temperature resistance, long-term high-pressure resistance, and excellent hot melt properties[8]. It has two advantages: stiffness (high modulus) and excellent long-term high-temperature creep resistance[9]. Furthermore, these unique structures can improve mechanical strength, creep resistance against external stresses, long-term hydrostatic strength, resistance to slow crack growth (SCG), and rapid crack propagation (RCP)[8,9].

Polymer-based nanocomposites have been explored extensively for the numerous innovative and remarkable features that nanoparticles can provide to polymers[9]. Graphene has attracted attention for its advanced thermal, mechanical, and optical properties, and one of its most important derivatives is graphene oxide (GO). Oxidation of graphite powder to GO is a well-established approach to generating graphene-based materials. The large surface areas of graphene make its nanocomposites more advanced materials[9,10]. Graphite oxide is prepared by intercalating and oxidizing graphite with mixtures of strong acids, introducing abundant oxygen-containing functional groups to the graphite layers by expanding the layer spacing[10].

Further exfoliation of graphite oxide by ultrasound in polar solvents produces GO, which can be considered an insulator and disordered analog of highly conductive crystalline graphene[13]. Recent studies have shown that GO is a promising material due to its high surface area and because it presents different functional groups of oxygen, such as carboxyl, carbonyl, epoxy, and hydroxyl groups, that allow its functionalization to become more effective when added to polymeric matrices[14]. GO is one of the most important graphene derivatives with a high negative charge density that can be prepared from graphite, offering an impressive price advantage over carbon nanotubes[15]. A recent study investigated the properties of PE-RT nanocomposites with 5.22 wt.% expanded graphene, and the mechanical strength showed an increase of 42%, from 16.84 MPa to 21.20 MPa[9]. Other research has reported an increase in Shore hardness of 12.5-14.5% in nanocomposites containing 0.01-0.1% by weight of carbon nanotubes functionalized with titanium stearate[6]. Finally, adding a small amount of graphene nanoplates (GNPs) to the PE-RT matrix showed that the GNPs acted as a nucleating agent, increasing the degree of crystallinity[9].

The present study focuses on assessing the impact of incorporating graphene oxide (GO) nanoparticles into PE-RT for potential application in oil industry risers. The current literature lacks comprehensive studies evaluating the effectiveness of nanocomposites based on the PE-RT polymer matrix with GO. Therefore, the primary objective of this work is to investigate how the incorporation of GO nanoparticles influences the properties of PE-RT. Specifically, this research aims to address the prevalent issue of swelling in PE-RT, a significant limitation that affects its suitability for various applications. The produced nanocomposites were characterized by thermal, mechanical and morphological properties. The resulting properties of PE-RT nanocomposites in fixed fractions (0.5, 1.0, and 2.0 wt.%) of GO loads obtained by exfoliation/chemical reduction of graphite oxide were compared. PE-RT/GO nanocomposites were prepared using the melt blending method. It is worth noting that although several studies in the literature explore polyolefins with GO, this is the first to examine the impact of GO on bimodal polyethylene technology, which has become a trend, particularly in barrier layers for flexible petroleum pipeline.

2. Experimental Procedure

2.1. Materials

Natural graphite flakes were supplied by Nacional de Graphite Ltda., Brazil, with carbon contents of 87-99% (Graflake 99550). Polyethylene of raised temperature resistance (PE-RT) INTREPID with a density of 0.950 g/cm^3 was supplied by Dow Chemical, USA. Sulfuric acid (H_2SO_4), nitric acid (HNO_3), sodium nitrite ($NaNO_2$), potassium permanganate ($KMnO_4$), and hydrogen peroxide (H_2O_2) were purchased from Sigma-Aldrich Brazil.

2.2. Graphene production by the modified Hummers method

The synthesis of oxidized graphene was carried out according to the literature[16]. A total of 5 g of graphite from Nacional de Grafite 99550 with an average particle size +50 mesh (> 300 μm) was used. The graphite flakes were transferred to a 1 L Erlenmeyer together with 4.5 g of sodium nitrite ($NaNO_2$) and 169 ml of sulfuric acid (H_2SO_4) under magnetic stirring for 3 h in an ice bath, initiating the graphite intercalation. In the intercalation step, the oxidation process started by slowly adding 22.5 g of potassium permanganate over 2 h to the reagent's container. After this period, the ice bath was removed, and stirring was continued for 7 days. Then, the exfoliation step began, dripping 605 ml of 5% H_2SO_4 for 3 h with magnetic stirring. Subsequently, the viscous solution was washed with a solution of 3% H_2SO_4 and 0.5% H_2O_2 (15.8 ml of H_2SO_4, 7.8 ml of H_2SO_4, and 476.4 ml of distilled water) with magnetic stirring for 12 h. Twelve washes were performed with a solution of 3% H_2SO_4 and 0.5% H_2O_2 using a centrifuge. Then, the material was centrifuged and washed with distilled water until pH 7. This process generated oxidized graphite. Then, the material was dried in an oven at 100 °C until constant mass, resuspended in an Erlenmeyer with 70% ethanol, and placed in an ultrasonic bath (37-45 kHz) for 24 h in order to exfoliate the oxidized graphite to obtain oxidized graphene (GO).

2.3. Preparation of PE-RT/GO nanocomposites

The polymer pellets and GO particles were previously dried at 80°C. The nanocomposites were obtained using an extruder (Mini Lab II Haake composer) with double interpenetrating screws. Unfilled PE-RT was also processed under the same conditions for comparison. The following processing conditions were adopted: 180 ºC, screw rotation speed of 100 rpm for 6 min of residence. Four formulations were prepared in the extruder, exemplified in Table 1.

Table 1. Formulations of the obtained nanocomposites.

Codes	Description
PE-RT	neat PE-RT, processed
IGO0.5	PE-RT + 0.5 wt.% GO
IGO1.0	PE-RT + 1.0 wt.% GO
IGO2.0	PE-RT + 2.0 wt.% GO

2.4. Characterization of samples

2.4.1. Thermogravimetric analysis (TGA)

Thermal stability was measured using thermogravimetric analysis (TGA) on a Q500 instrument, TA (USA), for PE-RT and the obtained GO nanocomposites at triplicate measurements carried out under a nitrogen atmosphere. All samples (about 8 mg) were analyzed in a TA Instruments Q 500 analyzer (USA). Samples were heated at 10 °C/min up to 700 °C. Measurements were carried out in duplicate under a nitrogen atmosphere. In the thermograms obtained, T_{onset} (initial degradation temperature), T_{max} (temperature of the maximum degradation rate) and residue at 700 °C were determined.

2.4.2. X-ray diffraction (XRD)

The samples' crystalline arrangement was evaluated using X-ray diffraction (XRD) on a Rigaku Miniflex (Japan). The samples' crystallinity index (CI) was calculated through deconvolution using the ratio between the area corresponding to the crystalline regions and the area of the amorphous halo according to Equation 1[17].

$$CI = \frac{A_c}{\left(A_c + A_a\right)} \quad (1)$$

Where CI is the crystallinity index, A_a is the amorphous halo area, and A_c is the area of crystalline peaks. The diffractometer operated with 40 kV and an electrical source of 20 mA. A scan was performed at 2θ in the 2 to 40° range, with a goniometer speed of 0.05°/min. The radiation used was CuKα of 1.5418 Å. The interplanar distance between layers (d) and mean crystallite size (L_c) values were calculated using Bragg's law and Scherrer's Equation, Equations 2 and 3[17], respectively.

$$n\lambda = 2d\sin\left(\theta\right) \quad (2)$$

$$L_c = \frac{K\lambda}{\beta\cos()} \quad (3)$$

Where n is the reflection order, the wavelength of the X-rays; d is the interplanar distance between the layers; θ is the Bragg diffraction angle; Lc is the average crystallite size; K is a form factor (0.9), and β is the full width at half maximum (FWHM).

2.4.3. Differential scanning calorimetry (DSC)

DSC differential scanning calorimetry tests on a TA Instruments Q1000 (USA) were used to determine the melting temperature (T_m), crystallization temperature (T_c), and degree of crystallinity (X_c) of pure HDPE and nanocomposites. DSC tests used 4 to 6 mg samples in an airtight aluminum container. Two heating steps were performed. The first run was applied to erase the thermal history of the polymer. Then, the sample was cooled to 25 °C at a rate of 10° C/min with nitrogen flow and then heated again at 10 °C/min to 250 °C. The T_m and T_c temperatures were measured from the second heating curve. The degree of crystallinity was calculated from the enthalpy of fusion (ΔH_m) value according to Equation 4.

For PE-RT, the theoretical melting value associated with the 100% crystalline polymer of 293 J/g was considered[17].

$$X_c = \Delta H_m / \left(\Delta H_m^{100} \times f\right) \times 100 \quad (4)$$

Where X_c is the degree of crystallinity, ΔH_m is the heat of the enthalpy obtained by analyzing the sample, ΔH_m^{100} is the theoretical melting enthalpy of the 100% crystalline material, and f is the polymer fraction in the sample.

2.4.4. Contact angle

The level of hydrophilicity of the samples was measured from the angle formed between the surface of the samples and one of the tangents of the water drop surface. Measurements were performed using a Ramé-Hart Model 250 room temperature goniometer (USA). Five drops of deionized water were deposited per sample, and the angle to the left and right sides of the drop was measured. Each measurement was performed every 0.2 s, totaling 100. The drops contained approximately 5.0 µL in volume. The images were captured by a computer connected to the system, which automatically calculated the angle value. The samples (0.1 mm thick film) were prepared in a hydraulic press at 180 °C for 6 min. Subsequently, they were cooled in a circulating bath at 30 °C.

2.4.5. Scanning electronic microscopy (SEM)

SEM analysis was used to observe the dimensions of the obtained GO and evaluate the cryofractured surface of the nanocomposites. The specimens were prepared in a hydraulic press at 180 °C for 6 min at a pressure of 69 MPa. Then, they were cooled in a circulating bath at 30 °C. Scanning electron microscopy (SEM) analysis of freeze-fractured (N_2 at -196 °C) surfaces previously coated with gold was performed using a Quanta FEG250/FEI (USA).

2.4.6. Shore D hardness

Analyzes were performed on a Shore type D hardness tester by Shore Instruments & MFG (Japan). Samples were prepared as ASTM D2240[15]. The dimensions of the samples were 5 × 5 mm with a minimum thickness of 6.4 mm, manufactured in a hydraulic press at a temperature of 180 °C. To reach the minimum thickness, five samples were stacked. Five measurements were taken for each sample, and the average value was considered according to the standard used.

2.4.7. Tension test

The mechanical tensile test was carried out according to the international standard ASTM D638 (Standard Test Method for Tensile Properties of Plastic)[13], with a type V specimen in a universal testing machine Emic model L 3000 with a 30 KN (USA) load cell with 10 mm speed/min, manufactured in a hydraulic press at 180 °C. Twelve specimens of each composition were analyzed. The results concerning the mean and standard deviation of valid specimens were presented.

2.4.8. Aging test

The aging test was carried out using test specimens manufactured following the international standard ASTM D638 type V (Standard Test Method for Tensile Properties of Plastic)[13], manufactured in a hydraulic press at a temperature of 180 °C. Samples with 1.0 wt.% graphene oxide were submerged in synthetic petroleum (70% heptane, 20% cyclohexane and 10% toluene by volume), according to ISO 23936-1[14], inside steel autoclaves with a total volume of 2 L at a constant temperature of 80 ˚C and a sample was removed every month of aging. The initial (standard) mass of the specimens was measured before being submerged in the synthetic oil for monthly comparisons and calculation of the swelling degree. Subsequently, the samples were cleaned and stored in a dry environment for 3 days before being weighed to evaluate the swelling degree. After each withdrawal, the samples were dried. The variation in mass concerning time in the specimens was monitored by weighing, and the swelling degree (α) was determined from Equation (5)[9].

$$\alpha = \Delta m / m_i \times 100 \quad (5)$$

Where Δm represents the variance in sample mass after immersion in synthetic oil in relation to the initial mass of the sample, and mi is the pre-test mass in grams.

3. Results and Discussion

3.1. Thermogravimetric analysis (TGA)

Monolayer graphene is a material that does not suffer degradation up to 700°C due to its high thermal stability[18]. Figure 1 displays the thermogravimetric curve (TG) and its derivative (DTG) of GO.

As evident from the thermogram, oxidized graphene (GO) exhibits an initial degradation stage occurring at temperatures below 125°C. This initial stage is associated with the release of moisture, attributed to the adsorption of H_2O molecules by the GO material. The second stage, between 125°C and 300°C, is related to the loss of unstable oxygenated groups that degrade at lower temperatures[19]. This is due to the pyrolysis of hydroxyl, carbonyl and carboxylic acid groups into CO and CO_2[20]. Finally, the third stage of degradation occurs continuously from 300°C to 700°C, and this is due to the presence of chemically linked oxygenated groups in graphene with greater stability than the molecules degraded in the second stage[19,20]. Oxygenated groups such as epoxides and hydroxyls, found in the graphene network domain that do not represent defects, are relatively easy to remove. In contrast, those at the edges representing

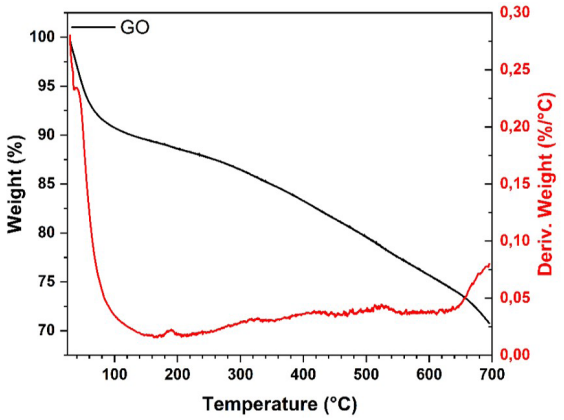

Figure 1. TG and DTG curves obtained from the GO sample.

significant defects are difficult to remove completely[20]. For more information about the graphene oxide produced, see the supplementary file.

Figure 2 displays the TG and DTG curves for pure PE-RT and its GO nanocomposites, and Table 2 provides the corresponding results.

Based on the findings, the matrix remains stable from room temperature up to 400 °C. Above 400 °C, its thermal decomposition accelerates significantly, with almost 95% mass loss occurring in a single event within the 450–500 °C temperature range. The highest mass loss rate was recorded at 480 °C, and at 500 °C, the remaining mass was slightly less than 3%. Additionally, the DTG graph shows the percentage of mass loss per unit of time as the temperature increases at a specific heating rate. This behavior has been observed in previous studies[18-21]. As expected, the degradation temperature is well above the working temperature. The purpose of the analysis was to verify whether oxygenated groups could favor degradation, not to achieve drastic improvements. Oxygenated groups could potentially act as fuel, enhancing degradation and significantly damaging the material. However, as observed in the TGA analysis, there was even a slight increase in thermal resistance, which is not always expected with the use of this type of particle. The TGA successfully evaluated the impact of GO on the thermal resistance of PE-RT, considering both theories mentioned. The good dispersion of GO, which has excellent thermal conductivity, likely helped with heat dissipation, thereby contributing favorably to the improvement of the thermal properties in question. Table 2 presents the results, including the temperature corresponding to 10% mass loss ($T_{10\%}$), the onset temperature of the degradation (T_{onset}), the temperature of the DTG degradation peak (T_{max}, representing the point at which the material degrades at the maximum rate), and the residue at 700 °C obtained from the thermograms. The incorporation of GO tended to elevate the degradation temperature of the materials, indicating that the nanoparticles enhance both the stability and thermal resistance of PE-RT.

Table 2. Results obtained by thermogravimetric analysis.

Sample	$T_{10\%}$ (°C)	T_{onset} (°C)	T_{max} (°C)	Residue (%)
PE-RT	431	446	474	0.07
IGO0.5	438	455	475	0.29
IGO1.0	442	458	477	1.02
IGO2.0	445	458	479	0.69

With the incorporation of 2 wt.% GO, the $T_{10\%}/T_{onset}$ increased from 431/446 °C to 445/458 °C, respectively. This indicates a notable enhancement in thermal stability, as evidenced by a 12 °C increase in the T_{onset} and a 14 °C rise in the $T_{10\%}$ for the composite with this specific composition. The incorporation occurs due to the impermeable nature of graphene oxide nanosheets. As a result, the pyrolytic products of volatile gas manipulation must diffuse around the nanoparticle/polymer interface instead of traveling straight through the polymer chain[21].

Thus, the tortuous gas diffusion paths through polymeric nanocomposites are increased, leading to a delay in the material degradation process, proving homogeneous distribution and effective interaction between PE-RT and GO[22]. Thermal degradation of PE-RT starts with C-C scission into radicals and then into the gas phase. The homogeneous distribution of GO in PE-RT and the strong interactions between them increase thermal conductivity, reducing the accumulation of heat in the polymer, thus not generating heat concentrating points that initiate the degradation of the material; that is, it delays degradation by distributing the heat better[23]. Moreover, it promotes the formation of a protective char layer, shown by the increase of residue content at 700 °C, similar to a network-state structure in preventing the exchange process of heat and degradation[24]. The results obtained by TGA indicate that the use of GO-based nanocomposites can be an economically promising strategy for the oil and gas industry, as the final product exhibits greater thermal stability compared to the pure polymer matrix used in the barrier layer, indicating a possible longer useful life of the riser.

3.2. X-ray diffraction (XRD)

Figure 3 shows the diffraction profiles of pure PE-RT and the GO nanocomposites produced. It is possible to observe a decrease in the intensity of the main polyethylene peak. It is worth mentioning that the diffractograms were not normalized

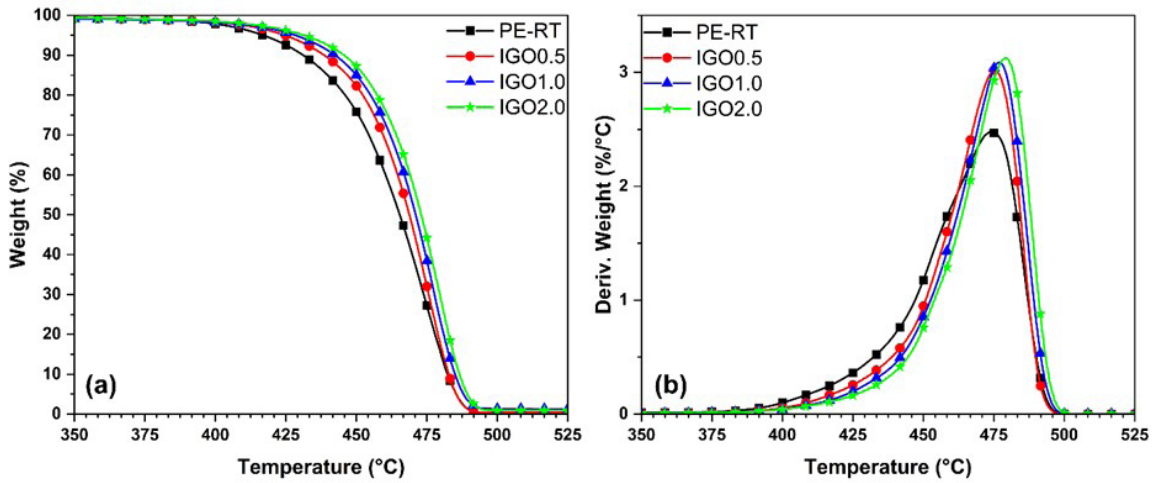

Figure 2. Comparison of TG (a) and DTG (b) curves between PE-RT and graphene oxide-based nanocomposites.

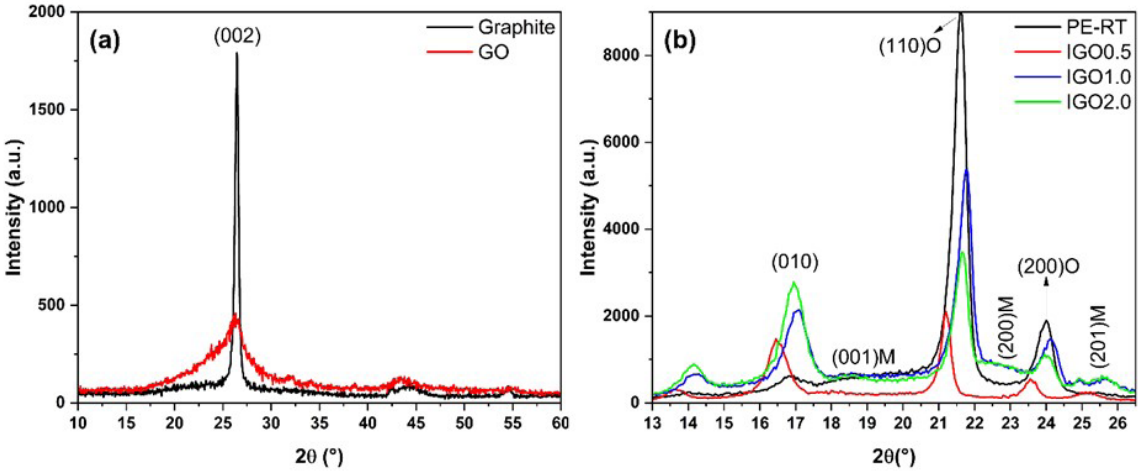

Figure 3. XRD profiles of graphite and GO (a) and PE-RT and nanocomposites incorporated with GO. M = monoclinic, O = Orthorhombic (b).

according to their maximum intensity. Additionally, the intensity observed can be closely associated with the sample quantity and the film thickness in the nanocomposites. The increase in crystallinity is accompanied by a reduction in the width of the crystalline peaks, demonstrating a significant reduction in the amorphousness of the material. This occurs because the amorphous regions scatter the X-rays more widely, without ordering, giving rise to the extended amorphous halo. Another contribution to the improvement of crystallinity is the increase in the intensity of crystallographic planes at smaller angles. Thus, when making the relationship between the crystalline areas in relation to the total, the constructive effects due to the insertion of GO generate a larger crystallinity index (CI). When graphite is transformed into graphite oxide, this peak is generally shifted to 11˚, and the peak at 26.5° has its intensity reduced and broadened due to the exfoliation of graphite into graphene oxide. The peak around 26.5° of graphite corresponds to a basal reflection (002) with d spacing of 3.363 Å, which is compatible with the literature data (JCPDS 75-2078, 3.347 Å)[25,26]. When graphite is oxidized and exfoliated using the Hummers method, the resulting nanolayers become intercalated, leading to network distortion, as documented in the literature (ICSD 1543272, representing a monoclinic symmetry and a lattice parameter of a = 12.42 Å, b = 25.15 Å, c = 6.28 Å, and β = 97.8°)[25,26]. Based on data from the literature and the results obtained from TGA, Raman and FTIR (Figure S1 and S2 of Supplementary material), it can be concluded that the graphite was effectively oxidized. Still, its structure was not completely compromised as the peak did not completely shift by 26.5°. Furthermore, a drastic reduction in intensity can be observed and, together with the broadening of the peaks and the SEM and Raman results (Figure S2 of supplementary material), it can be concluded that the GO was drastically exfoliated. The same diffractogram was recorded when GO was incorporated into the polymer matrix without any obvious peak at 11˚. This may indicate that graphite oxide was exfoliated into graphene oxide during the process and was very well mixed into the PE-RT matrix across all compositions[27].

The XRD pattern also shows two striking and distinct reflection peaks (110) and (200) appearing at 2θ = 21.5˚ and 2θ = 23.9˚, which correspond to interplanar spacings of 4.1 and 3.7 nm, respectively, typical of an orthorhombic unit cell of a polyethylene crystalline structure. Orthorhombic is the most stable phase at room temperature but also exists a small peak at 2θ = 19.5˚, which corresponds to the (001)M plane of the monoclinic phase (M), and two little evident peaks at 2θ = 23.2˚ and 2θ = 25.1˚, referring to the (200)M and (201)M planes[28].

Table 3. Crystallinity index (CI), interplanar distance (d_{110}), and the average size of crystals (Lc) in PE-RT and formulations based on graphene.

Sample	2θ (°)	d_{110} (nm)	Lc (nm)	CI (%)
PE-RT	21.57	0.41	17.6	45
IGO0.5	21.19	0.42	22.8	55
IGO1.0	21.72	0.41	17.8	42
IGO2.0	21.61	0.41	18.4	43

Table 3 displays the crystallinity index (CI), interplanar distance (d_{110}) and average crystallite size (L_c) values for the nanocomposites produced. The incorporation of GO tended to increase the CI of the matrix while also increasing the crystallite size, especially for the content of 0.5 wt.%. The IGO0.5% sample showed a shift of all diffraction peaks to smaller 2θ angles. It is believed that this concentration is still not enough to fill the polymer volume equally, presenting regions with lower GO contents or without the presence of such nanoparticles. Therefore, the GO nanolamellae tend to be located in regions with greater free volume in the polymer matrix, which is generally the amorphous region. However, there is also the possibility of more exfoliated nanosheets slightly increasing the interplanar distance of the crystallites. Two main theories could corroborate this phenomenon. The polymer crystallites could nucleate and grow on the surface of the corner of the most exfoliated GO nanosheets so that the planes are slightly further apart due to the separation at the edges of the crystal. The second theory would be that the oxygenated groups of GO would be responsible for the slight distortion. However, as observed in the diffractogram and by calculating $d_{110,}$ such variations are very small. They are considered to have a less significant influence

on the final properties of the materials than the increase in CI. Therefore, the nanoparticles promote increased crystal growth, as evidenced by the rise in CI and L_c. Compared to neat PE-RT, the L_c of the nanocomposites with 0.5 wt.% GO increased by approximately 5 nm. It implied that due to the addition of a low amount of GO nanoparticles, the lateral growth of the crystals along the (110) plane was promoted. At the same time, there is a sharp decrease in the intensity of the reflection and their half-widths in the 2θ region of 21.5˚, which indicates a change in their defectiveness[29]. The incorporation of GO into the matrix likely helped to reduce defects at the edges of the crystalline structures, resulting in narrower signals in the diffractogram, indicative of a more ordered material. Additionally, the narrow diffraction peak suggests a smaller discrepancy in the distribution of crystal sizes and structures with different interplanar distances, leading to a higher degree of ordering of the crystallites relative to the (110)O plane in the nanocomposite.

Increasing the GO content above 0.5 wt.% caused a slight reduction in the CI, which shows that the nanoparticles seem to decrease the mobility of the polymeric chains, thus reducing their organization and decreasing the crystallinity, which overcomes the nucleating effect of the nanofiller. The excess energy present at the interface between the polymer and GO likely serves as a driving force for crystal growth, as indicated by the observed increase in L_c. It suggests that the compatibility between the materials is somewhat good. In addition, as observed in the non-variation of the interplanar distance (d_{110}), it can be suggested that the nanoparticles did not deform or distort the polymer crystals concerning the plane (110), and probably the nanolaminates are lodged in the amorphous regions of the material. That is, the nanocomposites present crystals with similar perfection and quality.

In addition, the crystallographic plane that generates the signal around 16.8° has a wider interplanar distance than the planes with higher angles. As observed in the diffractogram, the incorporation of the GO in the polymer matrix has a significant effect on the organization of this plane. It is believed that for the same reason that nanolaminates are allocated in amorphous regions of greater free volume, they also orient the material in a way that favors crystallographic planes with greater interplanar distances. Namely, the phenomenon of GO intercalation in organized regions with greater spacing between them cannot be excluded either. It can also be speculated that nanoparticles prefer regions with greater free volume, and they end up ordering these structures, generating a certain organization, as observed by the increase in CI. At this point mentioned, it is only possible to observe very weak signals that may be related to the orientation of the nanolaminates due to the flow created by the extrusion, generating, in a way, signals related to the organization of the parallel laminae.

3.3. Differential scanning calorimetry (DSC)

The intrinsic structure of a semicrystalline polymer matrix such as PE-RT can significantly influence some properties of its nanocomposites, especially the mechanical performance and gas permeability of graphene-based materials. In this work, DSC studied the influence of GO nanoparticles on PE-RT non-isothermal crystallization processes and determined its thermal parameters. Figure 4 shows typical exothermic melting and crystallization curves of PE-RT samples and their nanocomposites.

The incorporation of GO does not significantly alter the T_c and T_m values of the nanocomposites compared to the polymeric matrix. That demonstrates that GO does not compromise the thermal transitions of the material, including the maximum working temperature. However, a noticeable increase is observed in the ΔH_m and X_c values of the samples containing 0.5 wt.% GO, indicating the obtaining of a material with greater organization and crystallinity. Samples with higher levels also showed a slight increase in ΔH_m. This demonstrates the enhancement of crystallinity due to the incorporation of GO. Table 4 displays the values of T_c (°C), T_m (°C), ΔH_m (J/g) and X_c (%) obtained.

The enhancement in X_c is attributed to the nucleation effect of the GO nanoparticles, which facilitates more efficient packing of the crystalline structure[30,31]. The uniform distribution of GO nanoparticles in the PE-RT matrix provides more nucleating surfaces, facilitating the involvement of numerous polyethylene molecules in the growth of the initial polymer nuclei with chain folding. This, in turn, further increases the

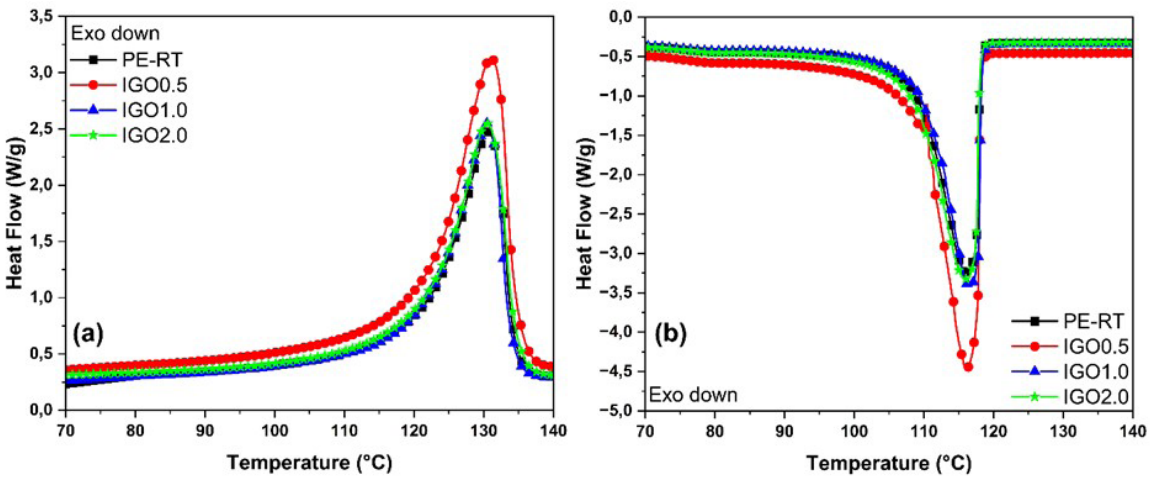

Figure 4. DSC curve for a sample of PE-RT and GO nanocomposites (a) melting; (b) crystallization.

Table 4. Results obtained by DSC analysis for the sample of PE-RT and its nanocomposites with GO.

Sample	T_c (°C)	T_m (°C)	ΔH_m (J/g)	X_c (%)
PE-RT	116.1	131	140	48
IGO0.5	116.2	131	184	63
IGO1.0	116.7	131	141	49
IGO2.0	116.2	131	149	52

Table 5. Contact angle of PE-RT and its GO-based nanocomposites.

Sample	Contact Angle (Degree)	Standard Deviation
PE-RT	98	0.27
IGO0.5	99	0.26
IGO1.0	100	0.26
IGO2.0	102	0.27

crystallinity. The divergence between these results and the crystallinity index calculated by XRD can be elucidated by the DSC method, which reveals a self-organization effect during heating, leading to an augmentation in the melting enthalpy and, consequently, in the degree of crystallinity. In other words, in DSC, thermally active crystals are observed, while in XRD, crystals with long-range organization are detected by diffraction. Above 0.5 wt.% GO, it can be seen that the improvement in crystallinity is not as significant. Likely, the well-dispersed GO sheets within the matrix inhibit crystal growth by confining the structure between the nanolaminate barriers.

3.4. Contact angle

Table 5 shows the mean contact angles obtained from PE-RT samples and their GO-based nanocomposites. The analysis of the contact angle in polymers is used to measure the water wettability in the sample. The investigated PE-RT has a contact angle of 98º, slightly above the value reported in the literature, 95.6º[30-32].

Adding higher GO contents in the nanocomposites gradually increased the contact angle. The addition of 2.0 wt.% GO resulted in a 4° increase in the contact angle compared to the pure polymer, indicating a slight enhancement in the material's hydrophobic character. The material used in the riser barrier layer must be resistant to water absorption, so greater hydrophobicity is expected to contribute to a better performance of PE-RT when used in flexible pipelines. A probable hypothesis is that the desirable contact angle for polymers used in risers is approximately 90°. If the material is too hydrophilic, it absorbs water, which facilitates PE-RT swelling and increases the permeability to water vapor, compromising the metal layers above the barrier layer and the integrity of the entire riser. Conversely, values significantly higher than 90° indicate a greater hydrophobic character and affinity for organic groups, which are unsuitable for risers as they can contribute to the formation of organic compound crusts and consequent clogging, impairing the flow of crude oil. The slight increase in the contact angle with the increase in GO filler content suggests good dispersion, the absence of nanoparticle agglomerates, and a surface with less roughness and high uniformity[33-40].

3.5. Scanning electronic microscopy (SEM)

Figure 5 shows the SEM image of graphene oxide using the method described previously.

The micrograph was taken at 30.0 kx magnification and shows that graphene oxide appears as aggregates of different dimensions. It is possible to observe that the morphology of these aggregates is formed by superimposed sheets or layers of GO. The layers do not have a regular organization, and the size is also heterogeneous. A similar morphology for GO has been reported in the literature, demonstrating that the Top-Down method of obtaining graphene oxide from the physical and chemical exfoliation of graphite generates heterogeneous structures with a variable lateral size distribution[41,42]. In the present work, it can be stipulated that the stacking of GO particles has a lateral size between 1-5 micrometers. Furthermore, as observed in microscopy, even the dry GO agglomerates, which are already expected, are much less than 0.1 micrometers thick (resolution limit of the scale used). Higher resolutions were limited due to the equipment available for use in the present study. It is universally known that when drying nanoparticles produced by liquid phase methods, the nanoparticles are agglomerated and reorganized when the solvent is removed. Therefore, when inserting such particles into the extruder, it is observed that such coarse agglomerates are broken down, enabling good dispersion in the polymeric matrix[43]. The process of extrusion of lamellar nanoparticles into polymeric frameworks can also inherently assist in the natural exfoliation of these structures, making them even more nanometric. Figure 6 shows the images of the cryogenic fracture surfaces of the polymeric matrix and the PE-RT/GO nanocomposites obtained by SEM with a magnification of 10,000x. The objective was to investigate whether the dispersion step was successful and the existence of clusters.

At this high magnification, it is possible to verify that the surface of the original sample (PE-RT) is rough, consisting of two phases, a dispersed one occluding a more continuous phase. It is, therefore, a heterophasic polyolefin, which can be explained by the presence of two main fractions with distinct molecular mass, as it is a bimodal polymer[44]. The surface of the cryofracture appears highly rough, indicative of irregular plastic deformation. Additionally, it can be observed that one phase fractured at a higher level than the other. The lower phase in the morphology shown in Figure 6a exhibits a smoother surface, characteristic of a fracture with minimal plastic deformation, while the higher region displays significant plastic deformation. This highlights the difference in mechanical properties between the phases of the bimodal polymer.

In this study was not possible to observe agglomerates of GO, and it was even difficult to identify the presence of this nanoparticle in cryofracture. This demonstrates the good dispersion of GO in the PE-RT matrix. The composite with 0.5 wt.% GO showed much smoother morphology, indicating the effect of filler reinforcement, even at low content. Furthermore, it can be suggested that GO helps distribute stress between the bimodal phases of the polymer, reducing the exaggerated plastic deformation of one phase in relation to the other. Even in nanocomposites with 2% GO by weight, it was difficult to identify the filler particles

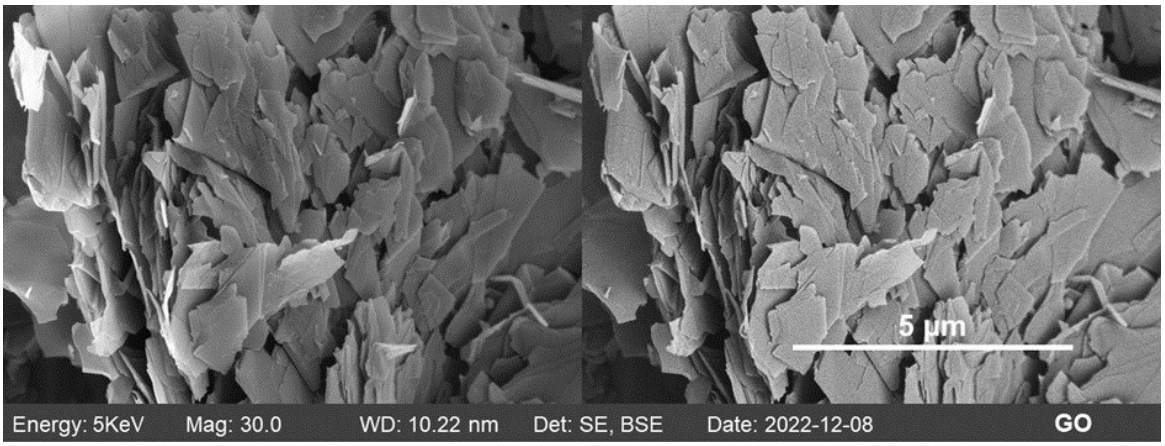

Figure 5. SEM images obtained for GO.

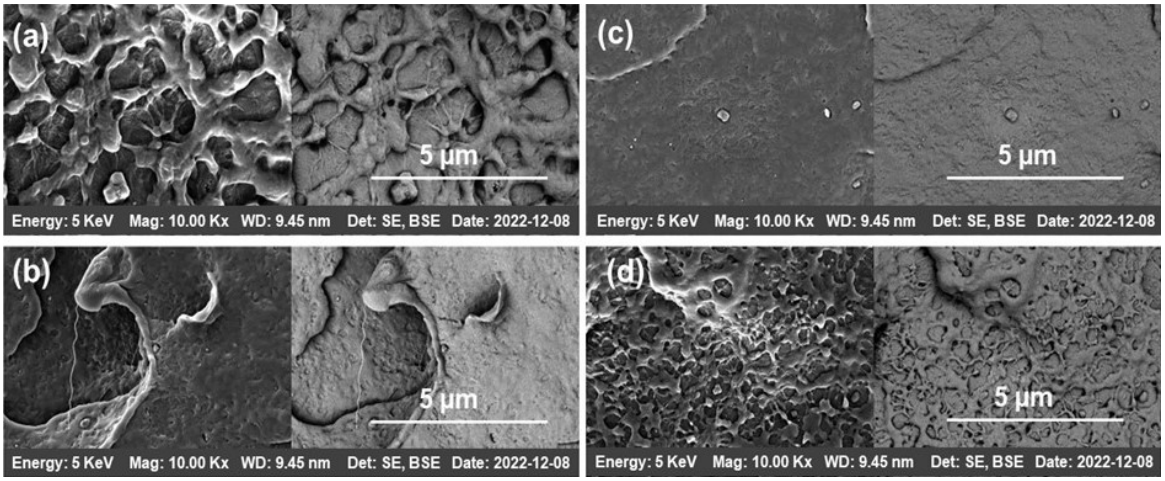

Figure 6. Images of the fracture surfaces of PE-RT and nanocomposites PE-RT/GO obtained in SEM: (a) PE-RT; (b) IGO0.5; (c) IGO1.0 and (d) IGO2.0.

on the cryofracture surface. This suggests that the extrusion process helped very well in the dispersion of the fillers and yet that the reinforcement phase presents good adhesion to the matrix[45]. Furthermore, it is worth mentioning that GO is a much better thermal conductor than the PE-RT matrix. Thus, the insertion of GO into the composites below the percolation threshold also favors better heat transfer in the nanocomposites. Above the percolation threshold, this effective transport effect may be questioned due to the continuous path of the load acting as an agglomeration and stress concentrator[43,46]. In nanocomposites with 2% GO, it is possible to observe that there is an indication of a process of creating roughness on the cryofracture surface, similar to the pure polymer. However, the surface does not present as drastic height variations as pure PE-RT. It can be suggested that from this concentration of GO (2.0 wt.%), load transfer starts to become less effective, generating heterogeneity due to excess filler. Finally, it is also believed that the extrusion process of GO nanoparticles in the PE-RT matrix can also help in the exfoliation of these lamellar structures, making them even more nanometric, corroborating the difficulty of identifying GO on the cryofracture surface[43]. The image of IGO1.0 suggests that the incorporation of 1.0 wt.% GO is a satisfactory balance between effort transfer, heat transfer and adequate filler concentration so as not to saturate any of the mechanisms that could harm the material's performance. The images show that the addition of this filler at low concentrations resulted in lower roughness of the material, suppressing the heterogeneous effect of the PE-RT bimodal composition. A more uniform surface was achieved up to 1.0% of GO, characterized by fewer imperfections or holes. This uniformity was due to improved dispersion of GO within the material, thereby contributing to enhancements in mechanical properties such as increased elastic modulus. Additionally, the uniform surface played a role in elevating thermal properties, leading to an increase in the material's ability to withstand higher temperatures.

3.6. Shore D hardness

The Shore D hardness test was conducted to evaluate possible changes concerning this characteristic regarding the matrix and the nanocomposites. The values obtained from pure PE-RT and nanocomposites are shown in Table 6.

Table 6. Shore D hardness values for PE-RT and nanocomposites.

Sample	Hardness	Standard Deviation
PE-RT	50	0.2
IGO0.5	53	0.2
IGO1.0	55	0.3
IGO2.0	59	0.1

Hardness measurement methods are the most common non-destructive tests for evaluating the mechanical properties of materials[47]. This is often used to study the mechanical properties of polymers. Hardness is a characteristic that expresses a material's resistance to deformation when subjected to a force concentrated on its surface[48].

It is possible to verify that, as expected, the addition of GO reinforcement increased the penetration resistance of the material. The nanocomposites showed an average increase of more than 3 Shore D hardness units, reaching 9 units more than pure PE-RT. That is because graphene oxide is a material of high hardness, transferring part of its characteristic to the polymeric matrix[49]. The results show that the incorporation of GO increases the hardness of the polymeric mixture, indicating good dispersion and homogeneity of the filler, leading to resistance to penetration by the needle of the instrument used, corroborating what is observed in the literature[50]. The increase in hardness of nanocomposites is attributed to the two-dimensional structure of GO, which is responsible for a very efficient transfer of forces during the indentation process, in which the applied force is predominantly transferred from the polymeric chains to the higher hardness structure of GO, preventing a deeper indentation on the surface of the nanocomposite[51].

3.7. Tension test

From the already mentioned investigations of nanocomposites, the good dispersion of GO in the PE-RT matrix can result in a potential reinforcement of the mechanical properties. The results were presented in a statistical format, with Table 7 specifically detailing the data in terms of the mean ± 95% confidence interval. It is possible to verify the tensile properties of the pure polymer compared with the nanocomposite with 1.0 wt.% of GO. The concentration of 1.0 wt.% GO was chosen because it improved the previously studied properties without compromising the material or causing surface roughness, as observed in the SEM analysis of the cryofracture surface. In contrast, the material with 2.0 wt.% GO showed surface irregularities due to excess GO. It is also believed that this concentration is already above the percolation threshold, which tends to compromise the performance of the nanocomposites under operation by requiring a set of thermal, mechanical and morphological properties. On the other hand, IGO0.5% exhibited lower improvements compared to IGO1.0%. Therefore, the material containing 1.0 wt.% GO was deemed the most promising for further study. Consequently, the tensile and aging tests were conducted exclusively on the IGO1.0% nanocomposites.

In addition, in Figure 7, the profile of the stress *vs*. strain curve of the PE-RT/GO nanocomposite with 1.0 wt.% of GO compared to the pure PE-RT can be observed.

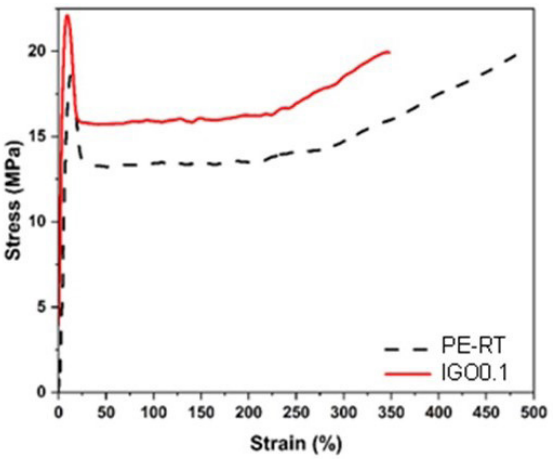

Figure 7. Stress *vs.* strain curve PE-RT pure and GO nanocomposite.

It is worth noting that the graph was plotted based on the curve that represents the specimen with median properties in relation to the population. Thus, as can be seen, some property values differ from the averages shown in Table 7. As the specimens are subjected to tension, the material initially responds with linear deformation, allowing for the calculation of Young's modulus at 0.2% strain. The stress-strain curve then reaches a maximum value, characteristic of the necking phenomenon, where the polymer chains are stretched, disrupting their conventional packing. Upon reaching the elastic limit, the polymer begins to deform plastically. During this phase, stress peaks are followed by a decline, resulting in a region of constant or slightly decreasing stress. This behavior indicates the onset of necking, which is characterized by a localized reduction in the cross-sectional area of the material. As deformation continues, this necking region elongates and propagates throughout the sample. After neck formation, deformation primarily occurs in the narrowed region, while the rest of the material remains relatively intact. Post-necking, the specimens reach a minimum in elongation, allowing for the reorganization of polyethylene chains. The stress level remains approximately constant up to 200-250% strain. During this phase, the material undergoes crystallization under tension, where the aligned chains reorganize into a crystalline structure. This enhances their resistance to further deformation, causing the stress-strain curve to rise until it reaches the strength limit of the chains, leading to failure.

Incorporating GO in the polymeric matrix made the material more resistant when verifying an increase in Young's modulus from 335 ± 37 MPa to 409 ± 42 MPa (22% increase). It means that higher stress is required for the material to deform. That is interesting for the application of the material since, under operation, it is not desired that the material changes its dimensions when subjected to tensile stresses. If the material undergoes variations along the force application axis, it would be possible for it to momentarily increase the free volume, which would reduce its barrier property to gases or even to swelling by liquids, possibly compromising the stability of the pipeline structure[52-54]. Furthermore, the reinforcing property added by GO can also be seen in the slight increase in stress at the yield point

Table 7. Statistical overview of tensile properties of composites with mean values and 95% confidence intervals.

Sample	Young modulus (MPa)	εy (%)	σy (MPa)	εr (%)	σr (MPa)
PE-RT	335 ± 37	13.3 ± 0.6	21.6 ± 1.4	496.0 ± 46.9	21.1 ± 1.5
IGO1.0%	409 ± 42	9.7 ± 0.5	22.1 ± 1.0	354.2 ± 59.8	18.4 ± 2.7

εy=elongation at the yield point; σy= stress at the yield point; εr = elongation at break; σr= stress at break

(σy). It demonstrates that the material in the elastic region tends to withstand greater tensions and, in the same way, a greater force would be required to deform it[55-58]. In addition, Figure 7 shows that the strain profile concerning the stress after the yield point tends to remain constant until a certain elongation. Then, the phenomenon of crystallization by stretching is observed[53]. It is characteristic of materials that, when stretched, end up with an alignment of the chains that promote compaction and crystallization, adding mechanical resistance to the material[54]. Another interesting detail is that in the plastic region, there was an increase in the material's mechanical strength due to the incorporation of nanoparticles. It is evidenced by the higher level after the yield point; the material requires greater stress to deform even with permanent deformation[55]. The reduction in elongation at break was already expected since the nanoparticles insert interfaces in the material, which present weaker interconnections in relation to polymer-polymer interactions[56]. It is common in nanocomposites because polymers generally have better compatibility with themselves than with other molecules due to the similarity of polarity and affinity of their chairs or tangles[57]. These interfaces also act as stress concentrators that behave as crack nuclei after extensive plastic deformation. In this context, the interface substantially retains the load subjected to the material, concentrating the energy mainly at specific points of the nanoparticle[58]. Thus, the plastic exceeds the activation energy required at a point of the nanocomposite, causing the phenomenon of crack propagation and the material fractures in smaller deformations[59]. This phenomenon of reduction of elongation also occurs in the elastic region when observing the reduction of elongation at the yield point (Ɛy). Graphene oxide nanosheets are generally lodged in the amorphous regions of the polymer because they have a greater free volume[60]. Thus, when the material is subjected to traction, it tends first to elongate those regions that present greater mobility caused by the free volume since the crystalline regions are more rigid[61]. Another fact is that the lamellar particles also cause spatial imprisonment in the chains, restricting their movement[62].

Considering only the results presented in this work, it can be suggested that the oxygenated groups of GO tend to favor a satisfactory interaction with the hydrogens of PE-RT, mainly in terms of nucleation and growth of crystals. The incorporation of GO tends to limit the stretching of PE-RT, restricting its deformation by confining the crystalline regions between the GO sheets dispersed in the matrix. Therefore, greater tensions are required to deform the polymer. Furthermore, the material will rupture at stress concentration points that will be at the interfaces of the GO nanosheets with the PE-RT. This is already expected to happen, as PE-RT has a stronger interaction with itself than with the nanoparticle. However, the reinforcement effects in the elastic region are those desired for the application, and it is in this region that the insertion of GO proves to be most advantageous (increase in Young's modulus and σy). Furthermore, it can be mentioned that, as observed in DSC, there is a slight increase in Xc, corroborating the reinforcement effect. The formation of a three-dimensional PE-RT network is an interesting suggestion, which goes hand in hand with the confinement of the crystallites by the GO nanosheets, thus favoring the mechanical properties mainly in the elastic region and also in a stress-strain curve above the pure polymer. It is important to note that excessive deformation beyond the elastic region during use is undesirable, as it can jeopardize the dimensional stability of the structure[63]. This property reduction is insignificant and does not compromise its application. The results of the mechanical tensile test indicated that the incorporation of GO enhanced the material's tensile properties.

3.8. Aging test

The aging of PE-RT occurs through a physical interaction where the synthetic oil penetrates the free spaces of the polymeric matrix, altering the material's structure[64]. Polymer degradation can be identified by swelling, increasing the geometry of the material and reducing its service life[65]. Pure samples of PE-RT and GO-based nanocomposites were carefully analyzed after being removed from immersion in synthetic oil, and no change in color and/or volume was observed.

Understanding the aging modes is important to prevent, control, and obtain a prognosis of when and how the material will fail. The swelling is generated by diffusion, that is, by installing the solvent in the polyethylene's free volumes (amorphous region)[64,65]. After the test period, it was verified that there was a greater mass increase in the unfilled samples compared to the nanocomposites, indicating that the addition of GO can effectively control the swelling of the PE-RT. Figure 8 compares the swelling degree of pure PE-RT samples and GO-based nanocomposites.

The swelling of polymeric materials is a phenomenon measured through the variation in mass related to the density or volume of the material due to the absorption of petroleum[46,66]. In this study, it was decided to compare the values of the initial mass of the samples before submersion in synthetic oil with values of the mass measured after removing each submerged sample. Likewise, it was also decided to conduct the aging test only with samples based on 1 wt.% GO due to the tendency for the formation of filler agglomerates from higher levels and because we believe that the lower content of GO used in this study is insufficient for possible conclusions. Finally, the values were calculated to obtain the swelling degree. Graphically, it is possible to observe that after the first two months of testing, the PE-RT samples exhibited a slight increase in mass and from the third month on, there was a marked increase in the swelling

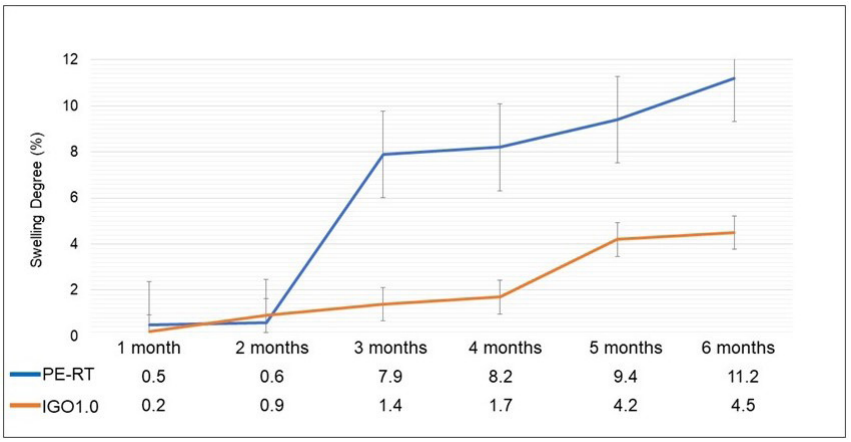

Figure 8. Swelling degree (α) of PE-RT and PE-RT/GO nanocomposite.

degree of the samples of 7.9; 8.2; 9.4 and 11.2% concerning the initial mass. Significant oil absorption occurs because polyethylene is a nonpolar polymer with a high affinity for hydrocarbons[46,67]. Nanocomposites provided better results than pure PE-RT, wherein the first three months of the test exhibited an increase in the swelling degree of only 1.4% relative to the initial mass (before immersion in synthetic oil). After a six-month immersion period, the samples containing GO exhibited a 4.5% increase in the swelling degree, which was significantly lower than observed in samples without additives. These findings suggest that GO demonstrates the potential to extend the lifespan of PE-RT by diminishing the void spaces between polymeric chains. This impediment to oil absorption and polymer swelling highlights the effectiveness of GO in enhancing PE-RT durability.

4. Conclusion

The results obtained in this work showed that the initial objectives were achieved. The incorporation of low amounts of graphene oxide (GO) into the polyethylene of raised temperature resistance (PE-RT) exhibited notable effects across various material properties. An increase in thermal degradation temperature was observed, indicating enhanced thermal stability. Concurrently, the Shore D hardness results revealed a proportional rise in sample hardness corresponding to higher filler contents. The GO nanoparticles notably influenced the crystallinity index and crystallite size, particularly evident at a 0.5 wt.% content. The contact angle values indicated a slight enhancement in hydrophobicity, especially at a 2.0 wt.% addition of GO. Although the 0.5 wt.% GO composition exhibits a higher degree of crystallinity, other properties such as thermal resistance, Shore D hardness, contact angle, dispersion, and homogeneity tend to improve with increasing nanoparticle content. Therefore, it can be concluded that the optimal concentration of GO in the PE-RT matrix is approximately 1.0 wt.%. Moreover, the concentration of 1.0 wt.% of GO increased Young's modulus of PE-RT, signifying improved mechanical strength. SEM imaging further depicted a remarkably smoother surface in the composite with 1.0 wt.% GO compared to the pure polymeric matrix. Remarkably, the nanocomposites displayed reduced swelling degrees than pure PE-RT, indicating the inhibitory effect of GO on material oil swelling. Overall, the findings underscore the superior thermal and mechanical properties of composites containing 0.5% and 1.0 wt.% of GO, presenting promising potential for application as flexible duct barriers.

Despite the high cost of GO as a nanofiller for PE-RT, it is important to note that the quantity required to produce the PE-RT/GO nanocomposite is very small. Even in this low quantity, significant improvements have been observed, especially for the barrier properties, the thermal degradation temperature, tensile strength, hardness and the material swelling degree. Therefore, the use of GO to produce the nanocomposite with this polymer matrix is justified, considering that it is cost-effective compared to other polymers used in barrier layers for risers.

5. Acknowledgments

This work was financially supported by CNPq, CAPES, and FAPERJ (Brazil). We also thank the CENPES laboratories for the equipment available for analysis.

6. References

1. Schramm D. PE-RT, a new class of polyethylene for industrial pipes. In: International Conference on Offshore Mechanics and Arctic Engineering (OMAE); 2006 Jan 4-9; Hamburg, Germany. Proceedings. New York: ASME; 2006.
2. Gobetti A, Ramorino G. Application of short-term methods to estimate the environmental stress cracking resistance of recycled HDPE. J Polym Res. 2020;27(11):353.
3. Zhan S, Xu H, Duan H, Pan L, Jia D, Tu J, et al. Molecular dynamics simulation of microscopic friction mechanisms of amorphous polyethylene. Soft Matter. 2019;15(43):8827-39.
4. Joshi NC, Gururani P. Advances of graphene oxide based nanocomposite materials in the treatment of wastewater containing heavy metal ions and dyes. Curr Res Green Sustainable Chem. 2022;5:100306.
5. Thejas R, Khan MI, Reddy S, Oreijah M, Guedri K, Bafakeeh OT, et al. A review on electrical and gas-sensing properties of reduced graphene oxide-metal oxide nanocomposites. Biomass Convers Biorefin. 2024;14(12):12625-35.

6. Feng W, Wang Z. Biomedical applications of chitosan-graphene oxide nanocomposites. iScience. 2022;25(1):103629.
7. Abouzeid RE, Owda ME, Dacrory S. Effective adsorption of cationic methylene blue dye on cellulose nanofiber/graphene oxide/silica nanocomposite: kinetics and equilibrium. J Appl Polym Sci. 2022;139(25):e52377.
8. Dacrory S, Hashem AH, Hasanin M. Synthesis of cellulose based amino acid functionalized nano-biocomplex: characterization, antifungal activity, molecular docking and hemocompatibility. Environ Nanotechnol Monit Manag. 2021;15:100453.
9. Tienne LGP, Candido LDS, Cruz BDSM, Gondim FF, Ribeiro MP, Simão RA, et al. Reduced graphene oxide synthesized by a new modified Hummer's method for enhancing thermal and crystallinity properties of Poly(vinylidene fluoride). J Mater Res Technol. 2022;18:4871-93.
10. Dan S, Bagheri H, Shahidizadeh A, Hashemipour H. Performance of graphene Oxide/SiO_2 nanocomposite-based: antibacterial activity, dye and heavy metal removal. Arab J Chem. 2023;16(2):104450.
11. Jones H, McClements J, Ray D, Hindle CS, Kalloudis M, Koutsos V. Thermomechanical properties of virgin and recycled polypropylene: high-density polyethylene blends. Polymers. 2023;15(21):4200.
12. Kiranakumar HV, Thejas R, Naveen CS, Khan MI, Prasanna GD, Reddy S, et al. A review on electrical and gas-sensing properties of reduced graphene oxide-metal oxide nanocomposites. Biomass Convers Biorefin. 2024;14(12):12625-35.
13. ASTM: American Society for Testing and Materials. ASTM D638: standard test method for tensile properties of plastics. West Conshohocken: ASTM; 2022.
14. ISO: International Organization for Standardization. ISO 23936-1: oil and gas industries including lower carbon energy: non-metallic materials in contact with media related to oil and gas production: part 1: thermoplastics. Geneva: ISO; 2022.
15. ASTM: American Society for Testing and Materials. ASTM D2240: standard test method for rubber property-durometer hardness. West Conshohocken: ASTM; 2017.
16. Deepak J, Adarsha H, Keshavamurthy R, Ramkumar NP. Analysis of thermal behaviour of carbon nanotubes-reinforced HDPE composites developed using FDM process. J Inst Eng India Ser D. 2024;105(1):425-37.
17. Diallo AK, Helal E, Gutiérrez G, Madinehei M, David E, Demarquette N, et al. Graphene: a multifunctional additive for sustainability. Sustainable Mater Technol. 2022;33:e00487.
18. Sui Y, Qiu Z, Liu Y, Li J, Cui Y, Wei P, et al. Ultra-high molecular weight polyethylene (UHMWPE)/high-density polyethylene (HDPE) blends with outstanding mechanical properties, wear resistance, and processability. J Polym Res. 2023;30(6):222.
19. Abdolahzadeh T, Morshedian J, Ahmadi S. Novel polyethylene/tungsten oxide/bismuth trioxide/barium sulfate/graphene oxide nanocomposites for shielding against X-ray radiations. Int J Radiat Res. 2023;21(1):79.
20. Albozahid M, Naji HZ, Alobad ZK, Wychowaniec JK, Saiani A. Thermal, mechanical, and morphological characterisations of graphene nanoplatelet/graphene oxide/high-hard-segment polyurethane nanocomposite: a comparative study. Polymers. 2022;14(19):4224.
21. Bajpai A, Sharma N, Dwivedi PK, Sharma R. Rapid fabrication of graphene layers over polymeric substrates using atmospheric pressure plasma jet. IEEE Trans Plasma Sci. 2023;51(3):726-32.
22. Bertulessi M, Bignami DF, Boschini I, Longoni M, Menduni G, Morosi J. Experimental investigations of distributed fiber optic sensors for water pipeline monitoring. Sensors. 2023;23(13):6205.
23. Noah PMA, Ohandja LMA, Medjo RE, Chabira S, Ebanda FB, Ondoua PA. Study of thermal properties of mixed (PP/EPR)/ABS with five model compatibilizers. J Eng. 2016;(1):8539694.
24. Dabrowski B, Zuchowska A, Kasprzak A, Zukowska GZ, Brzozka Z. Cellular uptake of biotransformed graphene oxide into lung cells. Chem Biol Interact. 2023;376:110444.
25. Dideikin A, Vul A. Graphene oxide and derivatives: the place in graphene family. Front Phys. 2019;6:149.
26. Marcano DC, Kosynkin DV, Berlin JM, Sinitskii A, Sun Z, Slesarev A, et al. Improved synthesis of graphene oxide. Washington, DC: American Chemical Society; 2010.
27. Dey TK, Jamal M, Uddin ME. Fabrication and performance analysis of graphene oxide-based composite membrane to separate microplastics from synthetic wastewater. J Water Process Eng. 2023;52:103554.
28. Amurin LG, Oliveira P, Pereira AFTS, Ribeiro NC, Rezende DB, Silva GG. Ultrahigh molecular weight polyethylene-reduced graphene oxide composite scaling up to produce wear resistant plates. Front. Carbon. 2023;2:1291283.
29. Guliyeva NA, Abaszade RG, Khanmammadova EA, Azizov EM. Synthesis and analysis of nanostructured graphene oxide. J Optoelectron Biomed Mater. 2023;15(1):23-30.
30. Kusano R, Kusano Y. Symmetric expressions of surface tension components. J Adhes. 2023;99(16):2381-401.
31. Li X, Willy HJ, Chang S, Lu W, Herng TS, Ding J. Selective laser melting of stainless steel and alumina composite: experimental and simulation studies on processing parameters, microstructure and mechanical properties. Mater Des. 2018;145:1-10.
32. Lin TH, Phat LN, Tu PM, Thang TQ, Khoa BDD, Lam CV, et al. Recycled polyethylene terephthalate fibers aerogels modified with graphene oxide for adsorption of methylene blue and coated with polydimethylsiloxane tetraethyl orthosilicate for oil removal. J Polym Environ. 2023;31(2):648-63.
33. Liu W, Wu X, Li Y, Liu S, Lv Y, Zhang C. Fabrication of silver ions aramid fibers and polyethylene composites with excellent antibacterial and mechanical properties. E-Polymers. 2022;22(1):917-28.
34. Mizera A, Manas M, Stoklasek P. Effect of temperature ageing on injection molded high-density polyethylene parts modified by accelerated electrons. Materials. 2022;15(3):742.
35. Mohamat R, Bakar SA, Mohamed A, Muqoyyanah M, Othman MHD, Mamat MH, et al. Incorporation of graphene oxide/titanium dioxide with different polymer materials and its effects on methylene blue dye rejection and antifouling ability. Environ Sci Pollut Res Int. 2023;30(28):72446-62.
36. Ben Mrad A, Sheibat-Othman N, Amorim APA, Rosario RL, McKenna TFL. Polyethylene slurries: swelling and solubility. Macromol React Eng. 2023;17(3):2300020.
37. Natrayan L, Kaliappan S, Hatti G, Patil PP, Gaur P, Manikandan T, et al. Influence the graphene filler addition on the tensile behavior of natural kenaf fiber-based hybrid nanocomposites. J Nanomater. 2022;2022(1):3554026.
38. Panasiuk K, Dudzik K, Hajdukiewicz G, Abramczyk N. Acoustic emission and K-S metric entropy as methods to analyze the influence of gamma-aluminum oxide nanopowder on the destruction process of GFRP composite materials. Materials. 2023;16(23):7334.
39. Singh DK, Verma RK. Development of reduced Graphene oxide modified ultrahigh molecular weight polyethylene (rGO/UHMWPE) based nanocomposites for biomedical applications. J Thermoplast Compos Mater. 2023;36(9):3516-51.
40. Tan SY, Chong WC, Sethupathi S, Pang YL, Sim LC, Mahmoudi E. Optimisation of aqueous phase low density polyethylene degradation by graphene oxide-zinc oxide photocatalysts. Chem Eng Res Des. 2023;190:550-65.
41. Tarani E, Arvanitidis I, Christofilos D, Bikiaris DN, Chrissafis K, Vourlias G. Calculation of the degree of crystallinity of HDPE/GNPs nanocomposites by using various experimental techniques: a comparative study. J Mater Sci. 2023;58(4):1621-39.

42. Thiyagu C, NarendraKumar U. Effect of graphene on thermal, mechanical, and shape memory properties of polyurethane nanocomposite. Appl Phys, A Mater Sci Process. 2022;128(10):937.
43. Honaker K, Vautard F, Drzal LT. Investigating the mechanical and barrier properties to oxygen and fuel of high density polyethylene-graphene nanoplatelet composites. Mater Sci Eng B. 2017;216:23-30.
44. Veiskarami A, Sardari D, Malekie S, Mofrad FB, Kashian S. Evaluation of dosimetric characteristics of a ternary nanocomposite based on High Density Polyethylene/Bismuth Oxide/Graphene Oxide for gamma-rays. Sci Rep. 2022;12(1):18798.
45. Zhang C, Zhao B, Ding L, Zhang D, Yang F, Xiang M. Influence of comonomer distribution on crystallization kinetics and performance of polyethylene of raised temperature resistance. Polym Int. 2019;68(10):1748-58.
46. Gardette M, Perthue A, Gardette JL, Janecska T, Földes E, Pukánszky B, et al. Photo- and thermal-oxidation of polyethylene: comparison of mechanisms and influence of unsaturation content. Polym Degrad Stabil. 2013;98(11):2383-90.
47. Tai Z, Chen Y, An Y, Yan X, Xue Q. Tribological behavior of UHMWPE reinforced with graphene oxide nanosheets. Tribol Lett. 2012;46(1):55-63.
48. Aliyu IK, Mohammed AS, Al-Qutub A. Tribological performance of ultra high molecular weight polyethylene nanocomposites reinforced with graphene nanoplatelets. Polym Compos. 2019;40(S2):E1301.
49. Ran W, Niu L, Wang Y, Lin N, Feng G, Lan H. Lifetime prediction method of pressured gas polyethylene pipes by strain-hardening modulus and tensile test. Appl Sci. 2023;13(13):7965.
50. Silva-Leyton R, Quijada R, Bastías R, Zamora N, Olate-Moya F, Palza H. Polyethylene/graphene oxide composites toward multifunctional active packaging films. Compos Sci Technol. 2019;184:107888.
51. Palza H. Antimicrobial polymers with metal nanoparticles. Int J Mol Sci. 2015;16(1):2099-116.
52. Potts JR, Dreyer DR, Bielawski CW, Ruoff RS. Graphene-based polymer nanocomposites. Polymer. 2011;52(1):5-25.
53. Mirabzadeh R, Parvaneh V, Ehsani A. Estimating and optimizing the flexural strength of bonding welded polypropylene sheets by friction-stir welding method. Proc Inst Mech Eng Part L J Mater Des Appl. 2021;235(1):73.
54. Ghabeche W, Chaoui K, Zeghib N. Mechanical properties and surface roughness assessment of outer and inner HDPE pipe layers after exposure to toluene methanol mixture. Int J Adv Manuf Technol. 2019;103(5-8):2207-25.
55. Schoeffl PF, Lang RW. Effect of liquid oilfield-related media on slow crack growth behavior in polyethylene pipe grade materials. Int J Fatigue. 2015;72:90-101.
56. Qi G, Yan H, Qi D, Li H, Kong L, Ding H. Investigations of polyethylene of raised temperature resistance service performance using autoclave test under sour medium conditions. E-Polymers. 2021;21(1):346-54.
57. Chervov AA, Dmitriev DV, Kostromin SV, Bronnikov SV. Polyethylene swelling in organic solvents and its influence on mechanical properties. Plasticheskie Massy. 2021;(3-4):13-4.
58. Pham DC, Sridhar N, Qian X, Sobey AJ, Achintha M, Shenoi A. A review on design, manufacture and mechanics of composite risers. Ocean Eng. 2016;112:82-96.
59. Wan C, Chen B. Reinforcement and interphase of polymer/graphene oxide nanocomposites. J Mater Chem. 2012;22(8):3637.
60. Nasir A, Kausar A, Younus A. Polymer/graphite nanocomposites: physical features, fabrication and current relevance. Polym Plast Technol Eng. 2015;54(7):750-70.
61. Kong L, Qi D, Li H, Ding N, Ge P, Xu Y, et al. Aging of polyethylene of raised temperature resistance pipe liner after a four-year service in a crude oil gathering system. J Fail Anal Prev. 2021;21(4):1323-30.
62. Ferry L, Sonnier R, Lopez-Cuesta JM, Petigny S, Bert C. Thermal degradation and flammability of polyamide 11 filled with nanoboehmite. J Therm Anal Calorim. 2017;129(2):1029-37.
63. Hocker SJA, Hudson-Smith NV, Smith PT, Komatsu CH, Dickinson LR, Schniepp HC, et al. Graphene oxide reduces the hydrolytic degradation in polyamide-11. Polymer. 2017;126:248-58.
64. Maïza S, Lefebvre X, Brusselle-Dupend N, Klopffer MH, Cangémi L, Castagnet S, et al. Physicochemical and mechanical degradation of polyamide 11 induced by hydrolysis and thermal aging. J Appl Polym Sci. 2019;136(23):47628.
65. Chowdhury T, Wang Q. Study on thermal degradation processes of polyethylene terephthalate microplastics using the kinetics and artificial neural networks models. Processes. 2023;11(2):496.
66. Deshoulles Q, Le Gall M, Dreanno C, Arhant M, Priour D, Le Gac PY. Modelling pure polyamide 6 hydrolysis: influence of water content in the amorphous phase. Polym Degrad Stabil. 2021;183:109435.
67. Reis TMC, Castro VG, Amurin LG, Silva GG. Graphene oxide dispersion in epoxy resin prepared by direct phase transfer from ethanol: rheology and aging. Composites, Part C: Open Access. 2023;10:100340.

Supplementary material

The following online material is available for this article:

Figure S1 - FTIR Spectrum of graphite and graphene oxide.

Figure S2 - Raman spectra of graphite and GO.